Paper
Int'l J. of Aeronautical & Space Sci. 17(2), 175–183 (2016)
DOI: http://dx.doi.org/10.5139/IJASS.2016.17.2.175

Quantitative Assessment of Variation in Poroelastic Properties of Composite Materials Using Micromechanical RVE Models

Su Yeon Han*, Sung Jun Kim and Eui Sup Shin*****

Department of Aerospace Engineering, Chonbuk National University, Jeonju 54896, Republic of Korea

Abstract

A poroelastic composite material, containing different material phases and filled with fluids, serves as a model to formulate the overall ablative behaviors of such materials. This article deals with the assessment of variation in nondeterministic poroelastic properties of two-phase composite materials using micromechanical representative volume element (RVE) models. Considering the configuration and arrangement of pores in a matrix phase, various RVEs are modeled and analyzed according to their porosity. In order to quantitatively investigate the effects of microstructure, changes in effective elastic moduli and poroelastic parameters are measured via finite element (FE) analysis. The poroelastic parameters are calculated from the effective elastic moduli and the pore-pressure-induced strains. The reliability of the numerical results is verified through image-based FE models with the actual shape of pores in carbon-phenolic ablative materials. Additionally, the variation of strain energy density is measured, which can possibly be used to evaluate microstress concentrations.

Key words: poroelastic properties, composite materials, micromechanics, finite element analysis

1. Introduction

The microstructures of poroelastic solid materials are known to directly influence their macroscopic properties [1]. For example, effective elastic moduli and poroelastic parameters depend strongly on the geometry and spatial distribution of the internal pores, the state of the constituent phases, and the porosity [2, 3]. Moreover, to formulate the poroelasticity of heterogeneous composite materials, a fundamental understanding of the correlation between microstructures and macroscopic properties is essential [4, 5]. This is also of importance in investigating failure modes due to microstress concentrations such as ply-lift and pocketing of ablative composites [6, 7]. Accordingly, quantitative evaluation of the effects of various microstructures is necessary for reliable and accurate characterizations of poroelastic properties.

There have been many analytical and experimental studies of the correlation between porosity and poroelastic properties. They attempted to describe this correlation by deriving formulas from micromechanical governing equations or to suggest empirical solutions [8-12]. For instance, Arnold et al. [8] presented an equation for the prediction of the Poisson's ratio for spherical porosity and isotropic materials. Herakovich and Baxter [10] used the generalized method of cells (GMC) to study the influence of pore geometry on the effective elastic properties and inelastic response of porous materials. Pal [12] developed four models for the elastic properties of pore-solid materials using the differential effective medium approach (DEMA). Despite these efforts, such studies are aimed mainly at uniform constituent materials and have some limitations in quantifying microstructural effects in their formulations.

Other researches using finite element (FE) models that consider the materials' microstructure have been conducted, allowing better analysis of the effects of porosity and pore shape on elastic properties [13-17]. Roberts and Garboczi [13, 15] used the FE method to study the influence of porosity and pore shape on the elastic properties of porous ceramics. Li et al. [16] proposed an FE approach using a simplified approximation for void geometry and a random distribution for both void sizes and their locations. However, those focus mainly on Young's modulus and Poisson's ratio, and do not

* Graduate Student
** Graduate Student
*** Professor, Corresponding Author: esshin@jbnu.ac.kr

Received: July 7, 2015 Revised: March 25, 2016 Accepted: April 6, 2016

http://ijass.org pISSN: 2093-274x eISSN: 2093-2480

deal sufficiently well with composite materials that consist of multiple phases. Although some efforts have been directed towards analyzing the elastic properties of multi-scale composite materials, they do not study the deviational characteristics caused by microstructures [18-20].

In this paper, the effect of internal microstructure on the variation in poroelastic properties of composite materials is evaluated quantitatively. In accordance with the porosity, a wide variety of micromechanical representative volume element (RVE) models including different shapes and arrays of pores are considered and used to analyze composites with reinforcement and porous matrix phases. To allow analytical investigation of microstructural effects on poroelastic characteristics, the average, maximum, and minimum values of the effective elastic moduli and pore-pressure-induced strains are measured using RVEs, respectively. The variation in the poroelastic parameters is calculated based on the measurements of those two factors. In addition, the micro and macroscopic values of strain energy density are analyzed quantitatively, which can then be used for evaluation of microstress concentration. The reliability of numerical results is confirmed through image-based FE models containing actual pore shapes in composite materials.

2. Poroelasticity of Composite Materials

In order to explain the thermomechanical state of porous composites, the elastic deformation, pore-pressure-induced strain, and thermal expansion should be included in the strain-stress relations. Therefore, the thermo-poro-elastic constitutive equation can be expressed in index notation as follows [1]:

$$\varepsilon_{ij} = S_{ijkl}(\sigma_{kl} + \pi_{kl} p) + \alpha_{ij}\theta_{+} \tag{1}$$

where S is the elastic compliance tensor, π is the poroelastic parameter which adjusts the effective stress due to pore pressure p, and α and θ_{+} are the coefficients of thermal expansion and temperature change, respectively. In the case of composite materials with three mutually orthogonal axes (x_1, x_2, x_3), Eq. (1) is expressed in matrix notation as follows:

$$\begin{Bmatrix} \varepsilon_1 \\ \varepsilon_2 \\ \varepsilon_3 \\ \gamma_{23} \\ \gamma_{13} \\ \gamma_{12} \end{Bmatrix} = \begin{bmatrix} \frac{1}{E_1} & -\frac{\nu_{21}}{E_2} & -\frac{\nu_{31}}{E_3} & 0 & 0 & 0 \\ -\frac{\nu_{12}}{E_1} & \frac{1}{E_2} & -\frac{\nu_{32}}{E_3} & 0 & 0 & 0 \\ -\frac{\nu_{13}}{E_1} & -\frac{\nu_{23}}{E_2} & \frac{1}{E_3} & 0 & 0 & 0 \\ 0 & 0 & 0 & \frac{1}{G_{23}} & 0 & 0 \\ 0 & 0 & 0 & 0 & \frac{1}{G_{13}} & 0 \\ 0 & 0 & 0 & 0 & 0 & \frac{1}{G_{12}} \end{bmatrix} \left(\begin{Bmatrix} \sigma_1 \\ \sigma_2 \\ \sigma_3 \\ \tau_{23} \\ \tau_{13} \\ \tau_{12} \end{Bmatrix} + \begin{Bmatrix} \pi_1 \\ \pi_2 \\ \pi_3 \\ 0 \\ 0 \\ 0 \end{Bmatrix} p \right) + \begin{Bmatrix} \alpha_1 \\ \alpha_2 \\ \alpha_3 \\ 0 \\ 0 \\ 0 \end{Bmatrix} \theta_{+} \tag{2}$$

where E, G, and ν are Young's modulus, shear modulus, and Poisson's ratio, respectively, which are the macroscopically-averaged effective elastic moduli of porous composites. The subscripts 1 and 2 indicate the in-plane directions, and the subscript 3 indicates the through-thickness direction. For orthotropic composites without loading in the x_2 direction, Eq. (2) reduces to

$$\begin{Bmatrix} \varepsilon_1 \\ \varepsilon_3 \\ \gamma_{13} \end{Bmatrix} = \begin{bmatrix} \frac{1}{E_1} & -\frac{\nu_{31}}{E_3} & 0 \\ -\frac{\nu_{13}}{E_1} & \frac{1}{E_3} & 0 \\ 0 & 0 & \frac{1}{G_{13}} \end{bmatrix} \left(\begin{Bmatrix} \sigma_1 \\ \sigma_3 \\ \tau_{13} \end{Bmatrix} + \begin{Bmatrix} \pi_1 \\ \pi_3 \\ 0 \end{Bmatrix} p \right) + \begin{Bmatrix} \alpha_1 \\ \alpha_3 \\ 0 \end{Bmatrix} \theta_{+} \tag{3}$$

Under the condition that only pore pressure is exerted on composite materials in order to obtain the poroelastic parameters, Eq. (3) is rewritten as follows:

$$\begin{Bmatrix} \pi_1 \\ \pi_3 \end{Bmatrix} = \begin{bmatrix} \frac{E_1}{1-\nu_{13}\nu_{31}} & \frac{E_3\nu_{13}}{1-\nu_{13}\nu_{31}} \\ \frac{E_1\nu_{31}}{1-\nu_{13}\nu_{31}} & \frac{E_3}{1-\nu_{13}\nu_{31}} \end{bmatrix} \begin{Bmatrix} \frac{\hat{\varepsilon}_1}{p} \\ \frac{\hat{\varepsilon}_3}{p} \end{Bmatrix} \tag{4}$$

where $\hat{\varepsilon}$ is the expanding deformation due to the pressure inside pores, called the pore-pressure-induced strain. In Eq. (4), precise measurements of the effective elastic moduli and the pore-pressure-induced strains are important for calculating poroelastic parameters. However, these factors are significantly affected by the configuration and arrangement of the pores in a matrix phase. RVE models with various microstructures must be constructed to quantitatively assess those effects on poroelastic characteristics.

3. Micromechanical RVEs

3.1 Simplified FE Models

In general, porous composites consist of a reinforcement (fiber) phase and a matrix phase in which pores are randomly distributed. Unit square RVEs with a porous matrix phase like that shown in Fig. 1 are modeled in the x_1-x_3 plane. The superscripts r, m, and p mean reinforcement, matrix, and pore, respectively. In view of the geometrical and loading symmetries, only one quarter of the model is considered and discretized. The upper and right boundaries of the quarter model are constrained to be straight after deformation.

Considering the shape and array of the pores, RVEs are classified into two types. That is to say, the pore configuration is simplified based on rectangles (RP-series) and circles (CP-series) for parametric study. In particular, the CP-series have two subtypes of pore arrangements according to whether pores are non-overlapped (CP-A/B/C) or overlapped (CP-D/E). Specific parameters of the CP-series such as radius (r^p) and the number (n^p) of pores, and uniform overlapped length (l_{OL}) are described in Tables 1 and 2. The minimum spacing between pores (l^p) is set to 0.01 m.

Figure 2 shows examples of micromechanical RVEs modeled with an FE analysis program, MSC Patran/Nastran. The volume fraction of the matrix phase is equal to that of the reinforcement phase (V^r=V^m). In the RP-series, finite elements are randomly eliminated from an original mesh in accordance with the porosity in the matrix phase (φ^m=0.1, ..., 0.5 with increment 0.1 for each step). With respect to five different amounts of porosity, a total of twenty-five FE models are used for poroelastic analysis. In the CP-series, five kinds of models are under consideration, as listed in Tables 1 and 2. As a result, a total of twenty-five FE models are created, which use 5,572 to 9,795 rectangular elements (Quad4).

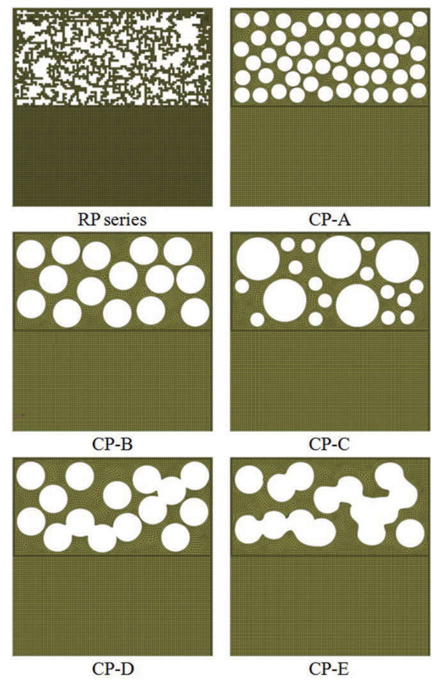

Fig. 2. Simplified FE models

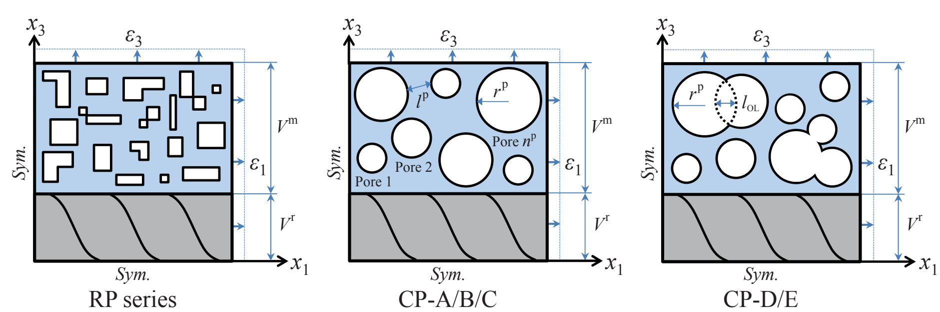

Fig. 1. Schematic of RVEs for two-phase (a reinforcement phase and a porous matrix phase) composite materials

Table 1. RVEs with non-overlapping circular pores

Porosity	CP-A		CP-B		CP-C			
	n^p	r^p [m]	n^p	r^p [m]	n_1^p	r_1^p [m]	n_2^p	r_2^p [m]
0.1	10	0.040	15	0.033	15	0.016	5	0.049
0.2	20	0.040	15	0.046	15	0.023	5	0.069
0.3	30	0.040	15	0.056	15	0.028	5	0.085
0.4	40	0.040	15	0.065	15	0.033	5	0.098
0.5	50	0.040	15	0.073	15	0.036	5	0.109

Table 2. RVEs with overlapping circular pores

Porosity	CP-D			Porosity	CP-E		
	n^p	r^p	l_{OL}		n^p	r^p	l_{OL}
0.100	15	0.033	0.01	0.094	15	0.033	0.05
0.200	15	0.046	0.01	0.190	15	0.046	0.05
0.298	15	0.056	0.01	0.287	15	0.056	0.05
0.393	15	0.065	0.01	0.374	15	0.065	0.05
0.497	15	0.073	0.01	0.463	15	0.073	0.05

3.2 Image-Based FE Models

In order to enhance the reliability of the numerical results using simplified FE models, image-based FE models with pore shapes similar to those of the actual pores in the matrix phase are also constructed. The process for image-based modeling has four steps, as shown in Fig. 3. Firstly, cross-sectional photographs of porous materials are taken with a microscope. Secondly, the cross-sectional photographs are transformed into binary images. Thirdly, text-formed images are obtained from binary ones by an image analysis program such as Image-Pro Plus v7.0. Also, the element numbers (pores in this case) can be extracted. Finally, the finite elements in the original micromechanical mesh are eliminated using extracted element numbers. In this paper, the cross-sectional photographs for image-based models are obtained from experimental data of carbon-phenolic ablative materials [21]. Fig. 4 shows all of the image-based FE models through the above steps, with porosities of 0.084, 0.225, 0.329, and 0.449, respectively.

4. Variation in Poroelastic Properties

For the purposes of this study, the variation in the effective elastic moduli, poroelastic parameters, and strain energy density is predicted using micromechanical FE models. The poroelastic properties of image-based FE models are also measured for reference values and are shown in Table 3. In all calculations, the elastic moduli of the solid phases are assumed to be E_1^r=100 GPa, $E_3^r = E^m$=15GPa, G_{13}^r=10GPa, and

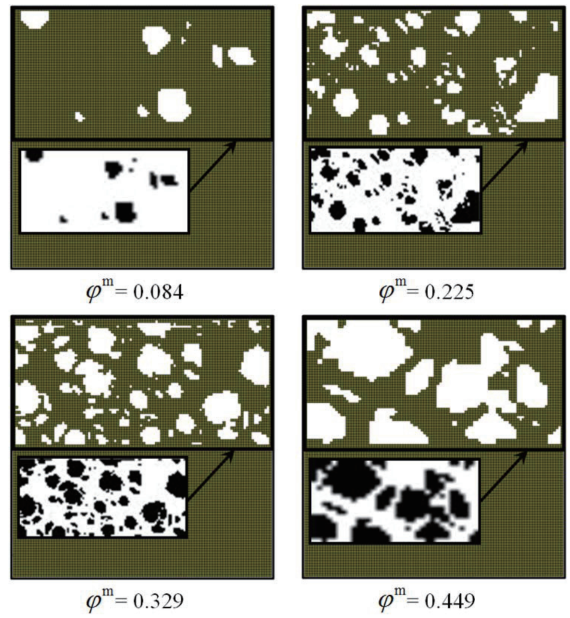

Fig. 4. Image-based FE models

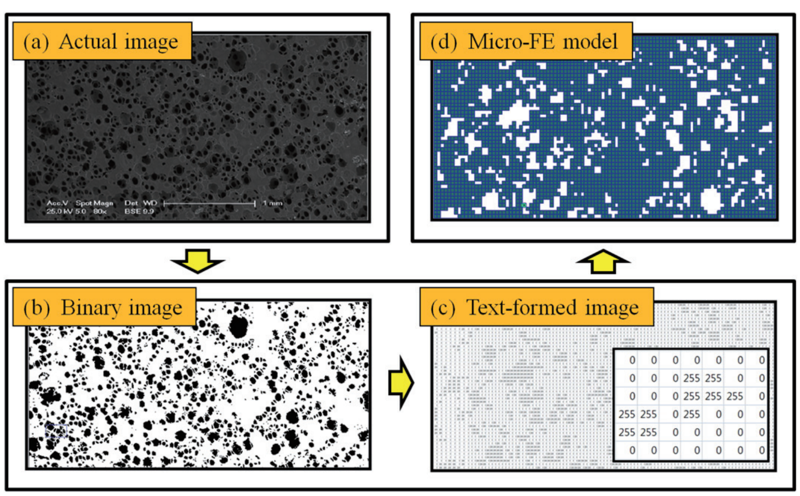

Fig. 3. FE modeling process based on photographic image data of porous materials

Table 3. Poroelastic properties of image-based FE models

Porosity	E_1 [GPa]	E_3 [GPa]	ν_{13}	$\hat{\varepsilon}_1$ [10^{-6}]	$\hat{\varepsilon}_3$ [10^{-6}]	π_1	π_3	W_{ave} [J/m^3]	W_{max} [J/m^3]
0.084	55.882	13.399	0.251	1.434	8.839	0.112	0.125	4.554	391.535
0.225	53.366	9.363	0.261	3.495	39.216	0.286	0.380	19.444	1542.105
0.329	52.416	4.744	0.289	4.083	70.855	0.340	0.474	33.523	2707.740
0.449	51.410	4.353	0.299	4.665	158.817	0.451	0.703	75.467	8295.725

DOI: http://dx.doi.org/10.5139/IJASS.2016.17.2.175

$\nu_{13}^{r} = \nu^{m} = 0.25$.

4.1 Effective Elastic Moduli

The variation in effective elastic moduli of porous composites is measured with respect to the porosity. To obtain these properties, uniform loading ($\bar{\sigma}_1$, $\bar{\sigma}_3$) is applied to the right or upper boundary in all FE models. As shown in Fig. 5, Young's modulus in the through-thickness direction E_3 decreases more rapidly than that in the in-plane direction E_1. With an increase in the porosity from 0.1 to 0.5, the average of E_3 decreases by 76.2% while that of E_1 decreases by 7.8%. Also, the effective elastic moduli of the RP-series are lower than those of the CP-series. It seems that the RP-series has more area surrounded by pores, which has a relatively lower load-carrying capacity. The variation in E_3 is higher than that in E_1: at a porosity of 0.5, the maximum variation in E_3 is approximately 84.8% from the average while that in E_1 is approximately 3.2%. Poisson's ratio, υ_{13}, is also plotted according to porosity. As the porosity increases, the average of υ_{13} decreases slightly, while the variation increases relative to the average. The quantitative results of effective elastic moduli with respect to each porosity are summarized in Table 4.

4.2 Poroelastic Parameters

In order to obtain the poroelastic parameters accurately, the pore-pressure-induced strain in each direction, $\hat{\varepsilon}_1$ and $\hat{\varepsilon}_3$,

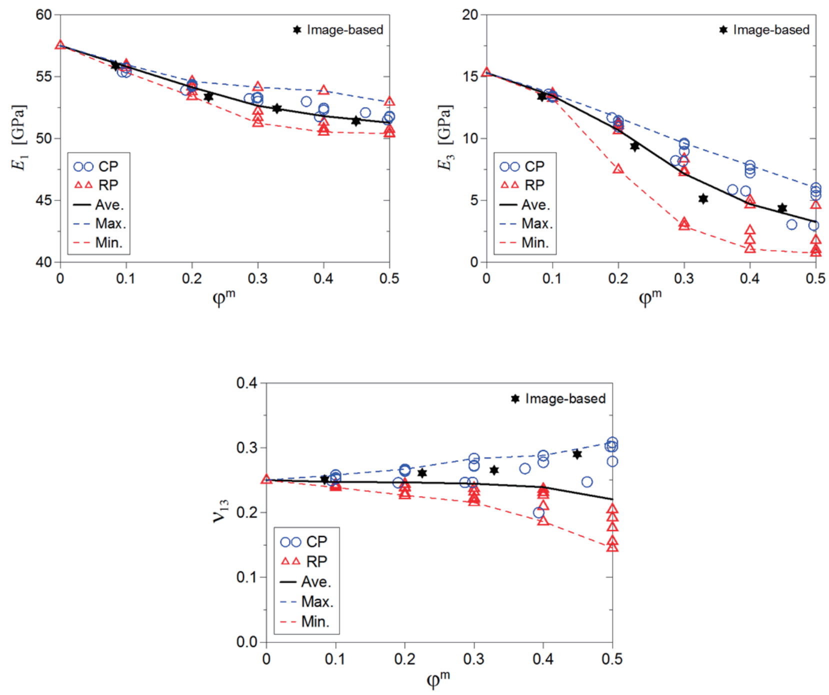

Fig. 5. Young's moduli and Poisson's ratio with respect to matrix porosity

Table 4. Variation in effective elastic moduli

Porosity	E_1 [GPa]		E_3 [GPa]		ν_{13}	
0.1	55.816	+0.3% -0.8%	13.445	+1.4% -1.6%	0.247	+4.4% -3.4%
0.2	54.134	+0.9% -1.4%	10.678	+9.4% -30.1%	0.247	+8.2% -8.1%
0.3	52.639	+2.8% -2.7%	7.149	+34.5% -59.6%	0.245	+15.9% -11.9%
0.4	51.808	+3.9% -2.5%	4.700	+66.4% -77.5%	0.239	+20.4% -34.7%
0.5	51.275	+3.2% -1.7%	3.255	+84.8% -77.7%	0.221	+39.8% -34.0%

is measured. As shown in Fig. 6, the average of $\hat{\varepsilon}_3$ increases much greater than does $\hat{\varepsilon}_1$: as the porosity increases from 0.1 to 0.5, $\hat{\varepsilon}_3$ increases by nearly 61-fold while $\hat{\varepsilon}_1$ increases by approximately 4-fold. Because pores are generated only in the matrix phase, the stiffness in the through-thickness direction decreases dramatically. In addition, the deformation in the in-plane direction is disrupted by the reinforcement phase. This leads to a difference in the pore-pressure-induced strain in each direction. The variation in $\hat{\varepsilon}_3$ is higher than $\hat{\varepsilon}_1$ as well: at a porosity of 0.5, the maximum variation in $\hat{\varepsilon}_3$ is approximately 137.5% from the average while that in $\hat{\varepsilon}_1$ is approximately 37.1%.

The poroelastic parameters are calculated by Eq. (4), which consists of the effective elastic moduli and the pore-pressure-induced strain. Fig. 7 shows that the average of the poroelastic parameter in the through-the-thickness direction, π_3, increases more rapidly than that in the in-plane direction, π_1: with an increase of the porosity from 0.1 to 0.5, π_1 is changed from 0.117 to 0.505, and π_3 is changed from 0.124 to 0.785. Also, the variation in π_3 is higher than that in π_1 as the porosity becomes larger. This is caused by two base factors. The poroelastic parameters in each direction are affected by the large directional differences of the effective elastic moduli and pore-pressure-induced strain. In addition, the distribution of pores oriented in the in-plane direction also causes directional difference in poroelastic parameters. The specific quantitative results are listed in Table 5.

4.3 Strain Energy Density

The distribution of microstress induced by pore pressure

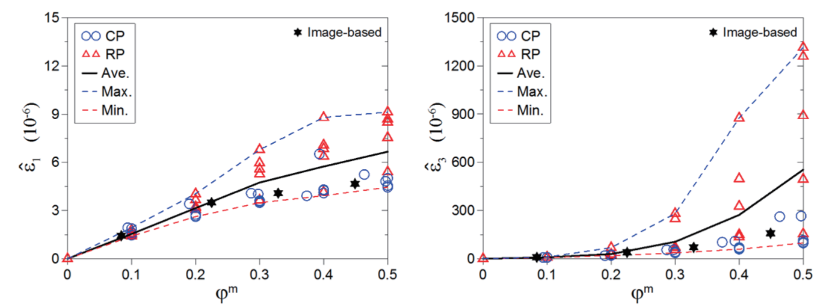

Fig. 6. Pore-pressure-induced strains with respect to matrix porosity

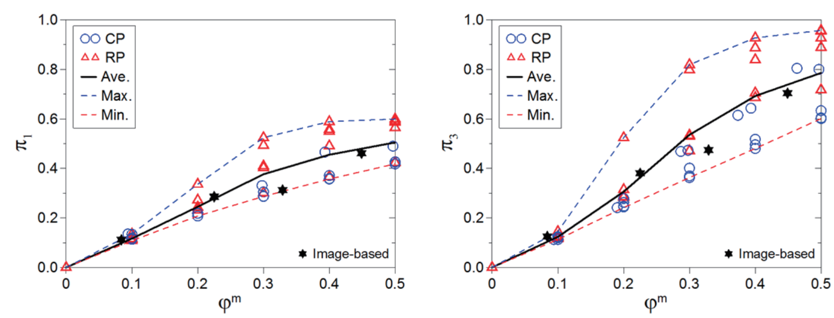

Fig. 7. Poroelastic parameters with respect to matrix porosity

Table 5. Variation in poroelastic parameters

Porosity	$\hat{\varepsilon}_1$ [10^{-6}]		$\hat{\varepsilon}_3$ [10^{-6}]		π_1		π_3	
0.1	1.541	+25.5% -8.9%	8.690	+19.7% -11.4%	0.117	+16.1% -7.3%	0.124	+17.4% -8.7%
0.2	3.149	+28.3% -16.8%	29.230	+135.1% -33.0%	0.245	+37.2% -15.3%	0.306	+71.2% -21.1%
0.3	4.739	+43.1% -26.4%	105.405	+166.7% -65.6%	0.376	+39.2% -23.8%	0.536	+52.9% -32.2%
0.4	5.735	+53.2% -31.7%	272.362	+221.5% -78.2%	0.455	+29.4% -21.5%	0.692	+34.0% -30.6%
0.5	6.658	+37.1% -33.2%	533.692	+137.5% -82.4%	0.505	+18.7% -17.2%	0.785	+21.9% -23.5%

DOI: http://dx.doi.org/10.5139/IJASS.2016.17.2.175

is one reason that progressive failure of porous composites occurs. The strain energy density can be used to evaluate the stress invariant rather than the individual stress components, and is expressed as follows [3]:

$$W = \frac{1}{2}\begin{Bmatrix}\sigma_1\\ \sigma_3\\ \tau_{31}\end{Bmatrix}_{\text{micro}}^{T}\begin{Bmatrix}\varepsilon_1\\ \varepsilon_3\\ \gamma_{31}\end{Bmatrix}_{\text{micro}} \tag{5}$$

where the subscript micro denotes microscopic values. The largest microscopic strain energy density is denoted by W_{max}. The macroscopically-averaged strain energy density W_{ave} is as follows:

$$W_{\text{ave}} = \frac{1}{2}\begin{Bmatrix}\sigma_1\\ \sigma_3\\ \tau_{31}\end{Bmatrix}_{\text{macro}}^{\text{T}}\begin{Bmatrix}\varepsilon_1\\ \varepsilon_3\\ \gamma_{31}\end{Bmatrix}_{\text{macro}} = \frac{\int_{\text{FE model}} W\, dV}{V} = -\frac{\int_{\text{All pores}} p u_n^{\text{p}}\, dS}{2V} \tag{6}$$

where V and u_n are the volume of a FE model and the outward normal displacement to the pore boundaries, respectively. The subscript macro also emphasizes macroscopic values, and the superscript p indicates pore-related values. As shown in Eq. (6), the stored strain energy in FE model is equal to the external work done by the pressure on the boundaries of all pores.

Depending on porosity, W_{ave} and W_{max} are measured considering various microstructures. As shown in Fig. 8, the average of W_{max} is much greater than that of W_{ave}. For example, at a porosity of 0.5, W_{max} is nearly 121-fold greater than W_{ave}, at 32994 and 272.7 J/m^3, respectively. In addition, as the porosity increases from 0.1 to 0.5, W_{max} increases 229-fold while W_{ave} increases 63-fold. These two values have a large variation due to microstructure, as shown in Table 6. Although W_{max}, a point value, depends on the fineness of the finite element mesh, the RP-series has a larger value than the others. This is confirmed by the distribution of the strain energy density in micromechanical FE models as shown in Fig. 9. They are selected from each type of RVEs shown in Fig. 2, and the image-based FE model, which has the largest W_{max}. In the RP-series, discontinuous solid phases are eliminated for the computational analysis by MSC Patran/Nastran. As expected, W_{max} is shown to be higher around pores as well as in narrower areas between pores.

5. Conclusion

The microstructural effects on the poroelastic characteristics of composite materials are quantitatively investigated using RVEs consisting of reinforcement and

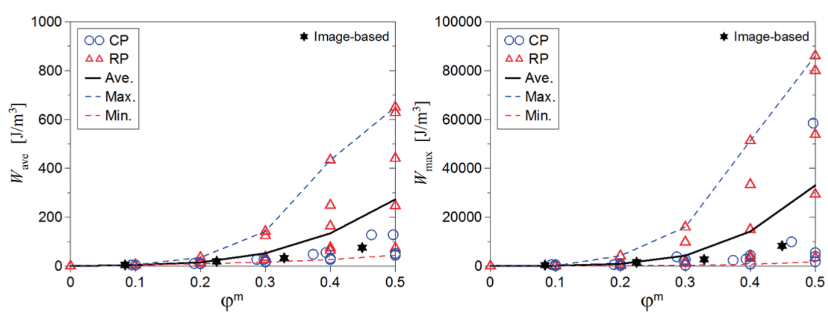

Fig. 8. Strain energy densities with respect to matrix porosity

Table 6. Variation in strain energy densities

Porosity	W_{ave} [J/m^3]		W_{max} [J/m^3]	
0.1	4.323	+27.3%	143.9	+139.6%
		-7.2%		-41.8%
0.2	14.53	+142.2%	896.2	+366.9%
		-35.8%		-83.5%
0.3	52.19	+171.5%	4244.	+276.0%
		-68.9%		-93.1%
0.4	134.0	+223.8%	14131.	+262.9%
		-80.2%		-95.1%
0.5	272.7	+138.5%	32995.	+160.8%
		-83.8%		-94.7%

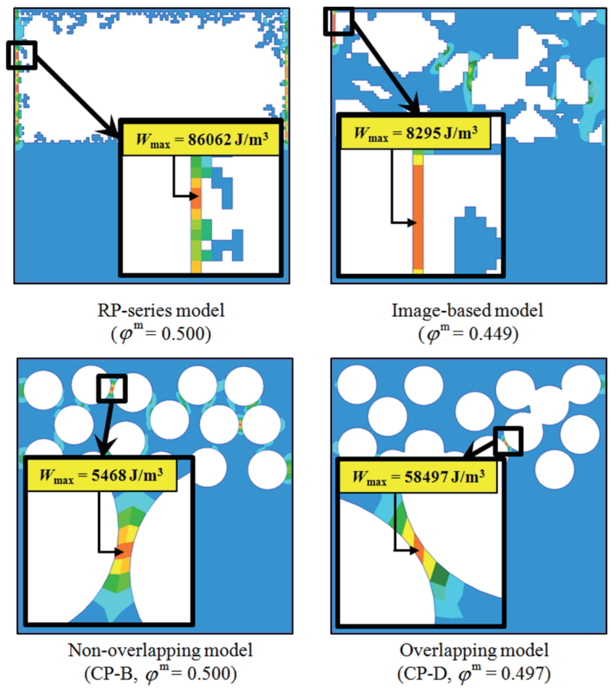

Fig. 9. Distribution of strain energy density

porous matrix phases. Considering the configuration and arrangements of pores, a variety of micromechanical FE models are created, and then analyzed to obtain numerical results. Image-based FE models with actual pore shapes are also used to confirm the reliable poroelastic properties. As a result, variations in effective elastic moduli and poroelastic parameter in the through-thickness direction are measured as higher than those in the in-plane direction since pores are intensively distributed in the matrix phase. In addition, the micro- and macro-scopic strain energy density varies greatly because of the configuration and arrangements of pores. All these results indicate that the microstructure of composite materials such as the geometric pore shape causes large variation in poroelastic properties. Therefore, in order to perform accurate and precise poroelastic analysis, the internal microstructure should be incorporated into FE models. Also, it is concluded that a statistical method is necessary to quantify microstructural effects.

Acknowledgement

This research was supported by Space Core Technology Development Program through the National Research Foundation of Korea (NRF) and funded by the Ministry of Science, ICT and Future Planning (MSIP) (NRF-2014M1A3A3A02034622).

References

[1] Coussy, O., *Poromechanics*, John Wiley & Sons, 2004.

[2] Kümpel, H. J., "Poroelasticity: parameters reviewed", *Geophysical Journal International*, Vol. 105, Issue 3, 1991, pp. 783-799.

[3] Kim, S. J., Han, S. Y. and Shin, E. S., "Micromechanics-based evaluation of poroelastic effect and stress concentration in thermochemically-decomposed composites", *J. of Mechanical Science and Technology*, Vol. 27, Issue 10, 2013, pp. 3139-3147.

[4] Li, S. and Wang, G., *Introduction to Micromechanics and Nanomechanics*, World Scientific Publishing Co., 2008.

[5] Ghoniem, N. M., Busso, E. P., Kioussis, N. and Huang, H., "Multiscale modelling of nanomechanics and micromechanics: an overview", *Philosophical Magazine*, Vol. 83, Issue 31-34, 2003, pp. 3475-3528.

[6] Wang, C. J., "The effects of resin thermal degradation on thermostructural response of carbon-phenolic composites and the manufacturing process of carbon-carbon composites", *J. of Reinforced Plastics and Composites*, Vol. 15, 1996, pp. 1011-1026.

[7] Bahramian, A. R., Kokabi, M., Famili, M. H. N. and Beheshty, M. H., "Ablation and thermal degradation behaviour of a composite based on resol type phenolic resin: process modeling and experimental", *Polymer*, Vol. 47, Issue

10, 2006, pp. 3661-3673.

[8] Arnold, M., Boccaccini, A. R. and Ondracek, G., "Prediction of the Poisson's ratio of porous materials", *J. of Materials Science*, Vol. 31, Issue 6, 1996, pp. 1643-1646.

[9] Cheng, A. H. D., "Material coefficients of anisotropic poroelasticity", *Int. J. of Rock Mechanics and Mining Sciences*, Vol. 34, Issue 2, 1997, pp. 199-205.

[10] Herakovich, C. T. and Baxter, S. C., "Influence of pore geometry on the effective response of porous media", *J. of Materials Science*, Vol. 34, Issue 10, 1999, pp. 1595-1609.

[11] Kováčik, J., "Correlation between Young's modulus and porosity in porous materials", *J. of Materials Science Letters*, Vol. 18, Issue 13, 1999, pp. 1007-1010.

[12] Pal, R., "Porosity-dependence of effective mechanical properties of pore-solid composite materials", *J. Composite Materials*, Vol. 39, No. 13, 2005, pp. 1147-1158.

[13] Roberts, A. P. and Garboczi, E. J., "Elastic properties of model porous ceramics", *J. of the American Ceramic Society*, Vol. 83, No. 12, 2000, pp. 3041-3048.

[14] Meille, S. and Garboczi, E. J., "Linear elastic properties of 2D and 3D models of porous materials made from elongated objects", *Modelling and Simulation in Materials Science and Engineering*, Vol. 9, No. 5, 2001, pp. 371-390.

[15] Roberts, A. P. and Garboczi, E. J., "Computation of the linear elastic properties of random porous materials with a wide variety of microstructure", *Proceedings of the Royal Society London* A, Vol. 458, Issue 2021, 2002, pp. 1033-1054.

[16] Li, B., Wang, B. and Reid, S. R., "Effective elastic properties of randomly distributed void models for porous materials", *Int. J. of Mechanical Sciences*, Vol. 52, Issue 5, 2010, pp. 726-732.

[17] Choi, H. K. and Shin, E. S., "Extended unmixing-mixing scheme for prediction of 3D behavior of porous composites", *J. of the Korean Society for Aeronautical and Space Sciences*, Vol. 41, No. 2, 2013, pp. 91-97.

[18] Kujime, T., Tane, M., Hyun, S. K. and Nakajima, H., "Three-dimensional image-based modeling of lotus-type porous carbon steel and simulation of its mechanical behavior by finite element method", *Materials Science and Engineering* A, Vol. 460-461, 2007, pp. 220-226.

[19] Sreeranganathan, A., Realistic micromechanical modeling and simulation of two-phase heterogeneous materials, *Ph. D. Dissertatio*n, Georgia Institute of Technology, 2008.

[20] Bar-On, B. and Wagner, H. D., "Effective elastic moduli of multi-scale composites", *Composites Science and Technology*, Vol. 72, Issue 5, 2012, pp. 566-573.

[21] Pulci, G., Tirillo, J., Marra, F., Fossati, F., Bartuli, C. and Valente, T., "Carbon-phenolic ablative materials for re-entry space vehicles: manufacturing and properties", *Composites Part A: Applied Science and Manufacturing*, Vol. 41, Issue 10, 2010, pp. 1483-1490.